Polarized Radiance Distribution Measurement of Skylight: Part 2, Experiment and Data

Yi Liu
Research and Data System Corporation
7833 Walker Drive Suite 550
Greenbelt, MD 20770

and Kenneth Voss,
Physics Department
University of Miami
P. O. Box 248046
Coral Gables, FL 33124

ABSTRACT

Measurements of the skylight polarized radiance distribution were performed at different measurement sites, atmospheric conditions, and three wavelengths using our newly developed Stokes polarimeter (RADS-IIP). Three Stokes parameters of skylight (I, Q, U), the degree of polarization, and the plane of polarization are presented in image format. The Arago point and neutral lines have been observed using RADS-IIP. Qualitatively the dependence of the intensity and polarization data on wavelength, solar zenith angle, and surface albedo is in agreement with the results from computations based on a plane parallel Rayleigh atmospheric model.

Key words: Stokes polarimeter, degree of polarization, neutral point, skylight

1. Introduction

Polarization is an intrinsic property of the light field. Solar radiation as a natural light source is not polarized before it enters the atmosphere. The natural light field is polarized

through scattering interactions[1,2] with the atmospheric constituents, such as the permanent gases (N_2, O_2, etc.), gases with variable concentration (O_3, SO_2, etc.), and various solid and liquid particles (aerosols, water, and ice crystals). The pattern of sky-light polarization[3] is related to the sun's position, the distribution of various components of the atmosphere, and the under-lying surface properties. Since the discovery of sky-light polarization by Arago in 1809, observations of sky-light polarization have been related to the studies of atmospheric turbidity[4,5,6] and surface properties.[7] The recent development of the Polarization Radiance Distribution Camera System[8,9] provides a new method to observe the sky-light polarization and can provide the spectral polarized radiance distribution over the whole hemisphere quickly and accurately.

It has been generally recognized that the principal features of the brightness and polarization of the sunlit sky can be explained in terms of Rayleigh scattering by molecules in the atmosphere.[3] Modern radiative transfer theory investigating polarization[1,2,10] has been applied to studies on planetary atmospheres[11,12] as well as the earth-ocean system.[13,14,15] Understanding the intensity and polarization of light in the atmosphere is also important in atmospheric correction of the remotely sensed data. The atmospheric correction algorithm developed for the Coastal-Zone Color Scanner (CZCS) imagery[16,17] is most easily understood by first considering only single scattering, including contributions arising from Rayleigh scattering and aerosol scattering. The analysis of multiple scattering effects was based on scalar radiative transfer computations in model atmospheres.[18] Recent advancements[19,20] solved the exact (vector) radiative transfer equation to compute the scalar radiance. Neglecting the polarization in radiance calculations in an atmosphere-ocean system will introduce errors as large as 30%.[21] Measurements of the total sky polarized radiance distribution can be used to test the validity of vector radiative transfer models. Through inversion techniques it can also be used in the determination of physical and optical properties such as the absorption and scattering phase function of aerosols[22] which

can not be done directly because of the difficulty in measuring the scattering phase function[23] and the single-scattering albedo.[24]

2. Background

Although scattering in the real atmosphere is more complicated than Rayleigh scattering, knowledge of the intensity and polarization of light in a plane parallel Rayleigh atmosphere is very important for discussion of the skylight. While quantitatively different, radiance distributions resulting from Rayleigh and Rayleigh-aerosol conditions exhibit similar variation with sun elevation, atmospheric turbidity and other parameters.[3]

A. Intensity of Skylight in a Model Atmosphere

To illustrate the dependence of the intensity of light in a model atmosphere on the surface properties, computations using Gordon's successive order approximation[19] (including polarization) in a Rayleigh atmosphere with a Fresnel reflecting surface was performed at a sun zenith angle of 53.1 degrees and at optical depths of 0.05, and 0.25. Light intensities on the principle plane are shown in Fig. 1 and compared with results from Coulson et al. [11] for the same atmosphere with a lambertian reflecting surface. The surface reflectances, R, are displayed on the graph. As can be seen, a Fresnel surface will increase the skylight intensity only slightly above a totally absorbing surface (R=0). A lambertian surface reflectance of 0.25 affects the radiance distribution much more, as will be seen in our experimental data.

In Fig. 1, the radiance has been normalized to the solar constant. It can be seen that the normalized radiance increases as the reflectance increases due to light being reflected from the surface. The normalized radiance also increases as the optical thickness increases. At this point it is worth noting that the separation between lines with different surface reflectances becomes larger as the optical thickness increases.

Since the skylight radiance for a clear atmosphere is dependent on both atmospheric turbidity and surface albedo, it is useful to look at the skylight measurements that have been made at various geographic locations and times. We have chosen cases in which cloud interference was absent or minimum.

B. Polarization of Skylight in a Model Atmosphere

The principal interest in measurements of skylight polarization is its sensitivity to dust, haze, and pollution in the atmosphere.[25,26] The maximum degree of polarization is diminished by the effects of aerosol scattering, and at the same time the neutral points (Q=0,U=0, defined below) of the polarization field are shifted from their normal positions. To illustrate how the degree of polarization and its maximum varies with surface properties and optical thickness, we will first look at computational results of a Rayleigh atmosphere using the plane parallel model.[3] These changes will be investigated with experimental data in next section.

Figure 2 illustrates the degree of polarization in the principal plane (azimuth angle 180 degrees) with a sun zenith angle of 53.1 degrees. The data were taken from tables computed by Coulson et al..[11] As can be seen, the degree of polarization has a strong dependence on surface properties and optical thickness. As the surface reflectance or optical thickness increases, the degree of polarization decreases accordingly. The Fresnel reflecting surface case was not shown, as the degree of polarization over a Fresnel reflecting surface is only slightly larger than that over a totally absorbing surface.

A convenient representation of the polarization of a light beam is the Stokes vector.[2] The four components of this vector, labeled I, Q, U, and V, are defined in terms of the electric field.[8,9] Simply these may be defined as:

$$I = I_l + I_r$$

$$Q = I_l - I_r$$

$$U = I_{45} - I_{135}$$

$$V = I_{rc} - I_{lc}$$

where I_l is the intensity of light polarized in a reference plane, I_r is the intensity of light polarized perpendicular to this reference plane, I_{45} and I_{135} is the intensity of light polarized in a plane 45 and 135 degrees to the reference plane, and finally I_{rc} and I_{lc} are the right and left circularly polarized intensities. Other parameters, used to describe the polarized light field, will be defined. The linear degree of polarization is defined as $\sqrt{(Q^2 + U^2)} / I$. The importance of the Stokes parameters Q and U in the atmosphere is that they define the polarization state of the atmosphere.

The neutral points are points where the degree of polarization is zero. Neutral points are then characterized by the double requirement Q=0 and U =0. For a lambertian surface these requirements are only met simultaneously at points on the principal plane. The Arago point is located above the anti-solar point. Two other points, the Babinet and Brewster points are located above and below the sun. Since the RADS-IIP instrument can not measure the part of the sky in which the Babinet and Brewster points occur due to an occulter, we will restrict our discussions to the Arago point. Neutral points can be outside the principal plane over a still water surface due to Fresnel reflections from the air-water interface.[27,28] Neutral points can also depart from their normal observed positions due to light scattering by dust, haze, and other aerosols[25], which suggest that neutral point positions are sensitive indicators of atmospheric turbidity.[3]

The lines which separate the regions of positive Q from the regions of negative Q are called neutral lines. Another parameter which can be deduced from the polarization field is the angle of the plane of polarization χ. χ, defined by $U = Q \tan(2\chi)$, is the angle between the plane of polarization and the vertical plane at the relevant azimuth. By symmetry, χ must be ± 90 degrees on the principal plane, depending on whether Q is positive or

negative, in either case U = 0. Also, when χ is zero, U is zero. Neutral lines, lines of U=0, and χ are particularly important to the examination of radiative transfer models.

3. Experiment and Data

A. Method of Measurement

The measurements of the polarization radiance distribution were all made with the Polarization Radiance Distribution Camera System (RADS-IIP)[8,9] at the following wavelengths: 439, 560, 667 nm. In normal operation, the analyzer is at each of three polarizer positions and an image obtained. The resulting data images, plus a dark count image taken with the shutter closed, constitute the basic data of one measurement. The overall time period for one complete measurement is 2 minutes. After correction for dark counts, the three data images are analyzed, and values of the Stokes vectors are computed and saved in image format. The degree of polarization and angle of the plane of polarization can also be calculated and displayed in image format. Measurement errors arise from errors in the recorded light intensity and the calibrated Mueller matrix elements. The uncertainties in recorded light intensities are due to (1) measurements taken in a series that extends about 1.5 minutes, ideally we should take measurements at the same time, and (2) unavoidable stray light and noise in the optical and electronic system. Normally skylight does not change significantly in 1.5 minutes especially when the sun elevation is high. Stray light and noise has been accounted for to the best of our abilities and as shown in comparisons with other instrument.[8] An analytical estimate shows the error in determination of the Mueller matrix elements can reach a maximum of 2%. To minimize the blooming effect caused by the direct solar radiation and the limited dynamic range of the system, a sun occulter has been adopted in our system to block the direct solar radiation.

This occulter also blocks a portion of the sky, as a result, there is a portion of the data not available on all data images on the sun's half of the atmosphere.

B. Description of Measurement Sites

The RADS-IIP polarimeter was deployed on top of JLK physics building on the main campus of University of Miami on Feb. 12, 1996 and on the top of the Science and Administration building (SLAB) at Rosenstiel School of Marine and Atmospheric Sciences (RSMAS) on Feb. 5, 1996 (at approximately 25° 43' N and 80° 16' W). The aerosol optical depths (AOD) for these days are shown in Fig. 3. The AOD measurements were made with a shadowband radiometer.[29] It can be seen that AOD varies with wavelength and time.

Feb. 12 was a very clear day and the surrounding area corresponds to a typical urban area. Buildings, vegetation, and surfaces of varied reflectances surround the site. Measurements taken on Feb. 5 have different features (Fig. 4), southeast of the site is water and northwest is land (including buildings, vegetation, and sand). On that day, there were clouds early in the morning and late in the afternoon, clear sky conditions occurred between 10:00 AM to 2:00 PM.

C. Radiance Distribution of Skylight

The data taken on Feb. 12 are shown first. In these cases, measurements of the sky radiance distribution were taken at 3 wavelengths (439, 560 and 667 nm) and typical data are shown in contour plots. Only 439 nm and 667 nm are shown for brevity. Figures 5a, 5b, and 5c are contour plots of radiance distribution at 439 nm (solar zenith angle 45.3°), 667 nm (solar zenith angle 47.2°), and 439 nm (solar zenith angle 77°) respectively. In these images the center is the zenith direction, the zenith angle is directly proportional to radius from the center. The bold circular lines are at 30 and 60 degree zenith angles. The units are 10^{-2} μW / (nm cm^2 sr). On the solar half of the hemisphere the rectangular area on the right of the image is the sun occulter, used to block the direct solar radiation.[8] In

general, for all three wavelengths, the minimum radiances appear on the antisolar half of the hemisphere. As the wavelength increases, the absolute values of the minimum region decreases. This reflects the wavelength dependence of Rayleigh scattering and explains the blue sky. It is important to note that the symmetry to the sun's principal plane exists in these images due to being over an approximately uniform reflectance background. One can also note the increase in radiance at the horizon due to the increased effective atmospheric path length at the horizon. As the sun-zenith angle increases, the absolute radiances decrease at all wavelength bands and the minimum regions shift with the sun.

Measurements were also performed on Feb. 5 on top of the Science and Administration (SLAB) building at RSMAS to investigate the effect of surface inhomogenities on the measurement. The major features are similar to the Feb. 12 data set. The area southeast of the measurement site at RSMAS is water and northwest is land. Feb. 5 was immediately after a cold front passed through Miami and the optical depths were higher than those on Feb. 12. It was cloudy early in the morning and late in the afternoon. Skylight intensity is significantly higher due to higher optical depth. Figure 6a is a contour plot of light intensity at 439 nm (solar zenith angle 46.3°) and figure 6b is at 667 nm (solar zenith angle 44.7°). On both graphs, the minimum intensity regions are shifted toward the direction over the water and thus destroy the symmetry to the principal plane. This shift from the principal plane decreases as the wavelength increases. The shift can be explained since a Fresnel reflecting surface (water) only increases the skylight intensity slightly but a surface with R=0.25 (approximates land) has a large effect (Fig. 1).

D. Stokes Parameter Q and Neutral Lines

Figures 7a -7c show the contour plots of the Stokes parameter Q for the images shown in Figs. 5a-5c. These demonstrate how Q changes with wavelength and sun angle. The numbers shown on the graphs are first normalized to the intensity and multiplied by 1000. They all show good symmetry to the principal plane as expected from a plane parallel

model and the uniform surface. The deviation from this symmetry mainly appears on the sun's half of the atmosphere. Neutral lines (designated with number 0) are formed clearly on the hemisphere opposite to the sun. Parts of neutral lines are also formed on sun's half of the atmosphere but large parts of these lines have been blocked due to the sun occulter. The minimum Q (negative number) appears on the principal plane and 90 degrees from the solar position. Tables 1 and 2 list the minimum Q's on the principal plane. Q is negative inside the neutral lines but positive outside and the maximum contours are symmetric to the principal plane and expand with the increasing solar zenith angle. As the solar zenith angle increases, neutral lines shrink significantly but still keep the similar shape and form a closed line. The contours crossing the principal plane seem to be dragged towards the zenith and their shapes change significantly.

E. Stokes Parameter U and Lines of U=0

Figures 8a - 8c show the contour plots of the Stokes parameter U for the images shown in Figs. 5a-5c. These demonstrate the change in U with wavelength and sun angle. The numbers shown on the graphs are first normalized to the intensity and multiplied by 1000. The Stokes parameter U is anti-symmetric to the principal plane, U=0 lines only appear on the principal plane and on the sun's half of the atmosphere. This is in agreement with the computation results using a plane parallel Rayleigh atmosphere model.[3] In the contour plots shown, since the sky in the vicinity of the sun has been blocked, a closed U=0 lines are not shown but the parts of lines shown suggest this trend. Again the deviation from anti-symmetry seems to occur on sun's side of the atmosphere. The maximum regions (both negative and positive) occur on the half of the atmosphere opposite the sun. As the solar zenith angle increases, these contours displace towards the zenith and their shapes are deformed. As the wavelength increases, for constant solar zenith angle, the maximum region expands, which implies larger degrees of polarization at longer wavelength. Table 3 lists the maximum U's. Notice that when the sun is low, the U=0 line on the principal

plane has deflected from a straight line and bends close to the horizon. This phenomenon is not seen in a Rayleigh scattering plane parallel model with a uniform surface. A possible explanation could be that water is southeast of the measurement site. As the sun was setting (west, azimuth angle around 247 degrees from true north for graphs shown) the U=0 lines shift towards the part of the atmosphere where the polarization is influenced by reflection from water. When the sun was high, the water body was under the sun's half of the atmosphere and had a negligible effect.

F. Degree of Polarization and Neutral Points

Figures 9a - 9c show the contour plots of the degree of polarization, P, for the images shown in Figs. 5a-5c. These demonstrate how P changes with wavelength and sun angle. The numbers shown on the graphs have been normalized to the radiances and then multiplied by a factor of 1000. The degree of polarization shows very good symmetry to the principal plane. Starting from the position of the sun (figure 9), the degree of polarization increases as the primary scattering angle increases. The maximum values occur in the region where the primary scattering angle is 90 degrees from the sun, this is in agreement with our earlier discussion using a plane parallel model. Following the maximum region, the degree of polarization decreases as scattering angle increases. The maximum degree of polarization is larger for longer wavelength. Since the Rayleigh optical thickness is smaller for longer wavelengths, light in the longer wavelengths suffers less multiple scattering thus a larger maximum degree of polarization.

Tables 4 and 5 lists the maximum P on the principal plane. As in the real atmosphere, light interacts with aerosol particles as well as molecules, the degree of polarization deviates from the predictions of a simple Rayleigh atmosphere model. As the solar zenith angle increases, while the maximum degree of polarization moves with the sun to maintain a scattering angle of 90 degrees, new contours are formed around a point on the principal plane at which a minimum value in degree of polarization is shown. This point is the

Arago point described later. As the solar zenith angle increases, the degree of polarization also increases for all three wavelengths in accord with the theoretical expectations.[11] Another feature of the contour plot at lower sun elevation is the deviation from symmetry, this could be caused by light reflected by the water and then scattered into the measurement site as compared with light reflected by land, as discussed earlier.

Figure 10 plots all Arago points observed at various sun angles and at three wavelength bands. The position of the neutral points are measured in angular distance from the antisolar point. It can be seen that this angular distance increases as the solar elevation increases. The observed neutral points are at larger angles than the positions computed using a Rayleigh atmosphere with a totally absorbing surface. In Fig. 10, the total optical depths are listed for each channel. The difference between the observed value and the computed value is due to light scattering by aerosols and surface reflections.

G. Plane of Polarization

Figures 11a -11 c show the contour plots of the angle of plane of polarization, χ, for the images shown in Figs. 5a-5c. The numbers shown on the graphs have been multiplied by a factor of 100. These contour plots can be best understood when compared with the corresponding Q and U plots shown. At first let us point out that the heavy lines on the principal plane are an artifact of the contour program. χ is antisymmetric to the principal plane thus on each side of the principal plane χ approaches either 90 degrees or -90 degrees. The contour program sees an abrupt change of 180 degrees when crossing the principal plane and adds many lines close to the principal plane. χ is ± 45 degrees at the neutral lines and zero at lines of U=0 except in the principal plane. As the wavelength changes, χ changes according to the changes of Q and U. As the sun's elevation decreases, the contour on the half of the hemisphere opposite the sun shrinks significantly

while the contour on the sun's side expands. When the sun is low, the Arago point appears and some contours will go into the neutral point.

H. Degree of Polarization Influenced by Measurement Site and Aerosols

As mentioned previously, the measurement site at RSMAS is special because the southeast is water but the northwest is land (Fig. 4). This results in a change in the skylight distribution (Figs. 6a, 6b). To illustrate how these factors affect the polarization, contour plots of the degree of polarization have been chosen at 439 (Fig. 12a), and 667 nm (Fig. 12b). Though the region where the maximum degree of polarization occurs is 90 degrees from the sun in general, the maximum in the region most likely affected by water has higher values than the region most likely affected by land. This deviation from symmetry is because the degree of polarization over a Fresnel reflecting surface is much higher than the degree of polarization over a Lambertian reflecting surface. As the wavelength increases, the degree of polarization increases also. Comparing Figs. 9a and 9b with Figs. 12a and 12b, the degree of polarization is much lower on Feb. 5 (Figs. 12a and 12b) than on Feb. 12 (Figs. 9a and 9b) due to the higher aerosol optical thickness. Light scattered by aerosols is not as highly polarized as in the case of Rayleigh scattering and adding aerosols will result in a higher chance of multiple scattering. Table 6 lists the maximum degree of polarization (P).

4. Conclusions

Although various aspects of the intensity and polarization in the sunlit atmosphere have been studied in the past, rapid measurements of the absolute skylight polarization radiance distribution over the whole hemisphere have not been possible previously. In this paper, measurements of skylight polarized radiance distribution were performed at different measurement sites, different atmospheric conditions, and three different wavelengths.

Qualitatively the radiance and polarization data are in agreement with the results from computations based on a plane parallel Rayleigh atmosphere model.

The ability of RADS-IIP to give polarization radiance distributions has great application potential in studies of atmospheric aerosols as well as radiative transfer problems in the earth-ocean system due to the fact that data can be taken in a short time thus changes in the atmosphere during measurement can be avoided. The neutral point (Arago point) appearing in the data suggests the potential to detect other neutral points if a smaller sun occulter is adopted. Since anomalous neutral point positions[28] have been predicted to occur over a still water surface, RADS-IIP can also be used to detect this effect. In the future, data will be compared with computed data based on realistic atmospheric models (including aerosols and surfaces) and used to validate the models and investigate the optical properties of aerosols.

Acknowledgments

The authors would like to acknowledge the support of the Ocean Optics Program at ONR, under grant N000149510309 and NASA under NAS5-31363. Also we would like to thank Dr. H. R. Gordon's support in computation and Mr. Judd Welton's support in optical depths' measurement. One of the authors, Yi Liu, would like to acknowledge University of Miami for providing University fellowship during the course of this work.

References

1. K. N. Liou, *An Introduction to Atmospheric Radiation*, Academic Press, Inc. (1980).

2. H. C. Van de Hulst, *Light Scattering by Small Particles*, Dover Publications, Inc. (1981).

3. K. L. Coulson, *Polarization and Intensity of Light in the Atmosphere*, A. DEEPAK publishing, Hampton, Virginia, USA. (1988).

4. H. H. Kimball, "The effect of the atmospheric turbidity of 1912 on solar radiation intensities and skylight polarization," *Bul. Mt. Weather Observatory*, **5**, 295-312 (1913).

5. T. Takashima, H. S. Chen, and C. R. N. Rao, "Polarimetric investigations of the turbidity of the atmosphere over Los Angeles," in T. Gehrels (ed.), *Planets, Stars, and Nebulae Studied with Photopolarimetry*, Univ. of Arizona Press, 500-509 (1974).

6. K. L. Coulson, "Characteristics of skylight at the zenith during twilight as indicators of atmospheric turbidity: I: Degree of Polarization," *Appl. Opt.*, **19**, 3469-3480 (1980).

7. K. L. Coulson, "The polarization of light in the environment," in T. Gehrels (ed.), *Planets, Stars, and Nebulae Studied with Photopolarimetry*, Univ. of Arizona Press, 444-471 (1974).

8. Y. Liu, "Measurement of the intensity and polarization of light in the atmosphere", Ph. D. dissertation, University of Miami (1996).

9. K. J. Voss and Y. Liu, "Polarized Radiance Distribution of Skylight: Part 1, System Description and Characterization," submitted to *Applied Optics*. (1997).

10. S. Chandrasekhar, *Radiative Transfer*, Clarendon Press, Oxford (1950).

11. K. L. Coulson, J. V. Dave, and Z. Sekera, *Tables Related to Radiation Emerging From a Planetary Atmosphere with Rayleigh Scattering*, University of California Press, Berkeley and Los Angeles (1960).

12. J. W. Chamberlain, *Theory of Planetary Atmospheres*, **22**, Int. Geophys. Series, Academic Press, New York (1978).

13. G. N. Plass and G. W. Kattawar, "Polarization of the radiation reflected and transmitted by the earth's atmosphere," *Appl. Opt.*, **9**, 1122-1130 (1970).

14. G. W. Kattawar, G. N. Plass, and J. A. Guinn, Jr. "Monte Carlo calculations of the polarization of radiation in the earth's atmosphere-ocean system," *J. Phys. Oceanogr.* **3**, 353-372 (1973).

15. G. W. Kattawar and C. N. Adams, "Stokes vector calculations of the submarine light field in an atmosphere-ocean with scattering according to a Rayleigh phase matrix: effect of interface refractive index on radiance and polarization," *Limnol. Oceanogr.*, **34**, 1453-1472 (1989).

16. H. R. Gordon, "Removal of atmospheric effects from satellite imagery of the oceans," *Appl. Opt.*, **17**, 1631-1636 (1978).

17. H. R. Gordon, J. L. Mueller, and R. C. Wrigley, "Atmospheric correction of Nimbus-7 Coastal Zone Color Scanner imagery," in *Remote Sensing of Atmospheres and Oceans*, A. Deepak, Ed. (Academic, New York), 457-483 (1980).

18. H. R. Gordon and D. J. Castano, "Coastal Zone Color Scanner atmospheric correction algorithm: multiple scattering effects," *Appl. Opt.*, **26**, 2111-2122 (1987).

19. H. R. Gordon and M. Wang, "Surface-roughness considerations for atmospheric correction of ocean color sensors. I: The Rayleigh scattering component," *Appl. Opt.*, **31**, 4247-4260 (1992).

20. H. R. Gordon and M. Wang, "Surface-roughness considerations for atmospheric correction of ocean color sensors. II: Error in the retrieved water-leaving radiance," *Appl. Opt.*, **31**, 4261-4267 (1992).

21. C. N. Adams and G. W. Kattawar, "Effect of volume-Scattering function on the errors induced when polarization is neglected in radiance calculations in an atmosphere-ocean system," *Appl. Opt.*, **32**, 4610-4617 (1993).

22. M. Wang and H. R. Gordon, "Retrieval of the columnar aerosol phase function and single-scattering albedo from sky radiance over the ocean: simulations," *Appl. Opt.*, **32**, 4598-4609 (1993).

23. M. Nakajima, M. Tanaka, M. Yamano, M. Shiobara, K. Arao, and Y. Nakanishi, "Aerosol optical characteristics in the yellow sand events observed in May 1982 at Nagasaki--Part II Models," *J. Meteol. Soc. Jpn*, **67**, 279-291 (1989).

24. H. E. Gerber and E. E. Hindman, eds., *Light Absorption by Aerosol Particles*, Spectrum, Hampton (1982).

25. Z. Sekera, "Recent developments in the study of the polarization of skylight," *Adv. in Geophys.*, **3**, 43-104, Academic Press, New York (1956).

26. K. Bullrich, "Scattered radiation in the atmosphere and the natural aerosol," *Adv. in Geophys.*, **10**, 99-260, Academic Press (1964).

27. R. S. Fraser, "Atmospheric neutral points over water," *J. Opt. Soc. Am.*, **58**, 1029-1031 (1968).

28. R. S. Fraser, "Atmospheric neutral points outside of the principal plane," *Contrib. Am. Phys.*, **54**, 286-297 (1981).

29. J. J. Michalsky, R. Perez, and R. Stewart, "Design and development of a rotating shadowband radiometer solar radiation/daylight network," *Solar Energy*, **41**, 577-581. (1988)

Figure Captions

Figure 1. Normalized radiance on the principal plane with an azimuth angle of ϕ=180° and solar zenith angle of 53.1°. Data are shown for two optical depths, 0.05 and 0.25. Data with Lambertian surface are from Coulson et al.[11]

Figure 2. Degree of polarization at various optical depths, from Coulson et al.[11]

Figure 3. Aerosol optical depth (AOD) as a function of time on Feb. 5 and Feb. 12, 1996.

Figure 4. Illustration of the measurement site at RSMAS, used on Feb. 5, 1996.

Figure 5. Contour plots of skylight radiance. The data shown were taken on top of the JLK physics building at University of Miami on Feb. 12, 1996. The origin of the coordinate shown corresponds to the zenith and the inner and outer circles to 30° and 60° zenith angles respectively. (a) Measurement wavelength is 439 nm, solar zenith angle is 45.3 degrees, AOD(410 nm) is 0.17. (b) Measurement wavelength is 667 nm, solar zenith angle is 47.2 degrees, and AOD(410 nm) is 0.20. (c) Measurement wavelength is 439 nm, solar zenith angle is 77 degrees, and AOD(410 nm) is 0.14.

Figure 6. Contour plots of skylight radiance. The data shown were taken on top of the Science/Administration building at RSMAS on Feb. 5, 1996. (a) Measurement wavelength is 439 nm, solar zenith angle is 46.3 degrees, and AOD(410 nm) is 0.35. (b) Measurement wavelength is 667 nm, solar zenith angle is 44.7 degrees, and the AOD(410 nm) is 0.30.

Figure 7. Contour plots of the Stokes parameter Q. The measurement descriptions for a, b, and c correspond to 5a, 5b, and 5c respectively.

Figure 8. Contour plot of the Stokes parameter U. The measurement descriptions for a, b, and c correspond to 5a, 5b, and 5c respectively.

Figure 9. Contour plots of the degree of polarization. . The measurement descriptions for a, b, and c correspond to 5a, 5b, and 5c respectively.

Figure 10. The observed angular distance of the Arago point from the antisolar point versus solar elevation. Data obtained on Feb. 12, 1996.

Figure 11. Contour plots of the plane of polarization. The measurement descriptions for a, b, and c correspond to 5a, 5b, and 5c respectively.

Figure 12. Contour plots of the degree of polarization. The measurement descriptions for a and b correspond to 6a and 6b, respectively.

Table 1 The minimum Q/I (x1000) on the principal plane as a function of solar-zenith angle, θ_o, at 439 nm.

θ_o	40°	42.5°	44.5°	45.3°	52.6°	64.8°	69.3°	73.9°	77.1°
Q/I	406	438	467	535	546	564	570	569	592

Table 2 The minimum Q/I (x1000) on the principal plane.

solar zenith Angle(θ_o)	Q/I for 439 nm	Q/I for 560 nm	Q/I for 667 nm
45°	–535	–578	–584
75°	–592	–646	–638

Table 3 List of the maximum U/I (x1000).

solar zenith angle (θ_o)	U/I for 439 nm	U/I for 560 nm	U/I for 667 nm
45°	540	594	610
75°	580	640	630

Table 4 The maximum P (x1000) on the principal plane as a function of solar -zenith angle, θ_o, at 560 nm.

θ_o	40°	41.8°	43.9°	46.4°	53.5°	66°	70.1°	74.5°	77°
P	494	468	460	578	624	630	647	633	646

Table 5 List of the maximum P (x1000) on the principal plane.

solar zenith angle (θ_o)	P for 439 nm	P for 560 nm	P for 667 nm
44°	535	578	584
75°	592	646	638

Table 6 Illustration of the maximum degree of polarization (θ_o=45°). PP represents principal plane, MP represents the maximum P in the image.

Date, region	AOD at 410 nm	P at 439 nm	P at 560 nm	P at 667 nm
Feb. 12, PP	0.20	535	578	584
Feb. 5, PP	0.35	301	355	420
Feb. 5, MP	0.35	400	456	510

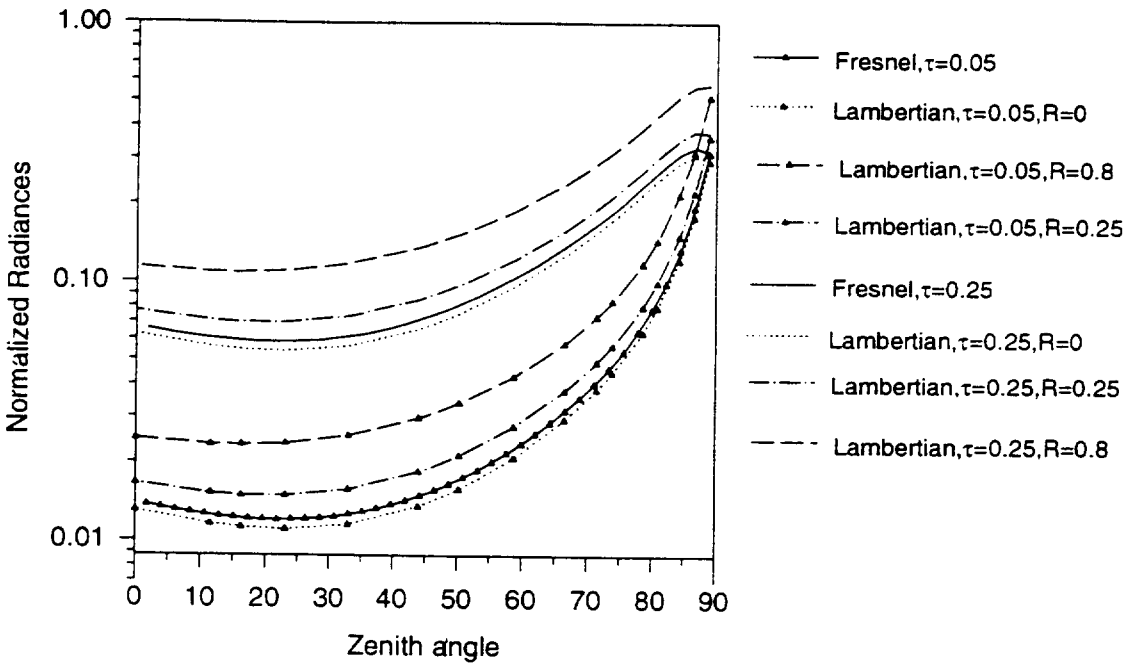
1.00
0.10
0.01
Normalized Radiances
0
10
20
30
40
50
60
70
80
90
Zenith angle
Fresnel,τ=0.05
Lambertian,τ=0.05,R=0
Lambertian,τ=0.05,R=0.8
Lambertian,τ=0.05,R=0.25
Fresnel,τ=0.25
Lambertian,τ=0.25,R=0
Lambertian,τ=0.25,R=0.25
Lambertian,τ=0.25,R=0.8

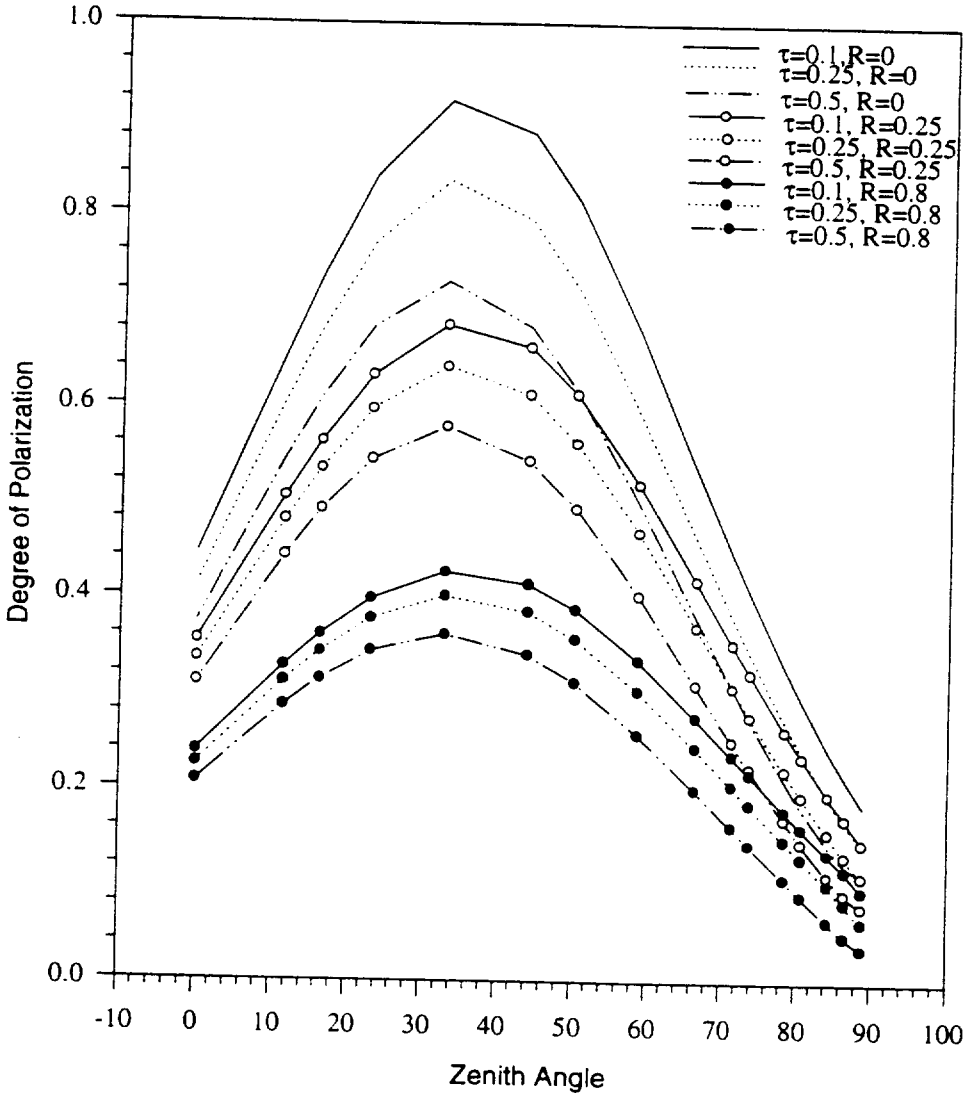

Fig. 6.7 Degree of polarization at various optical depths.

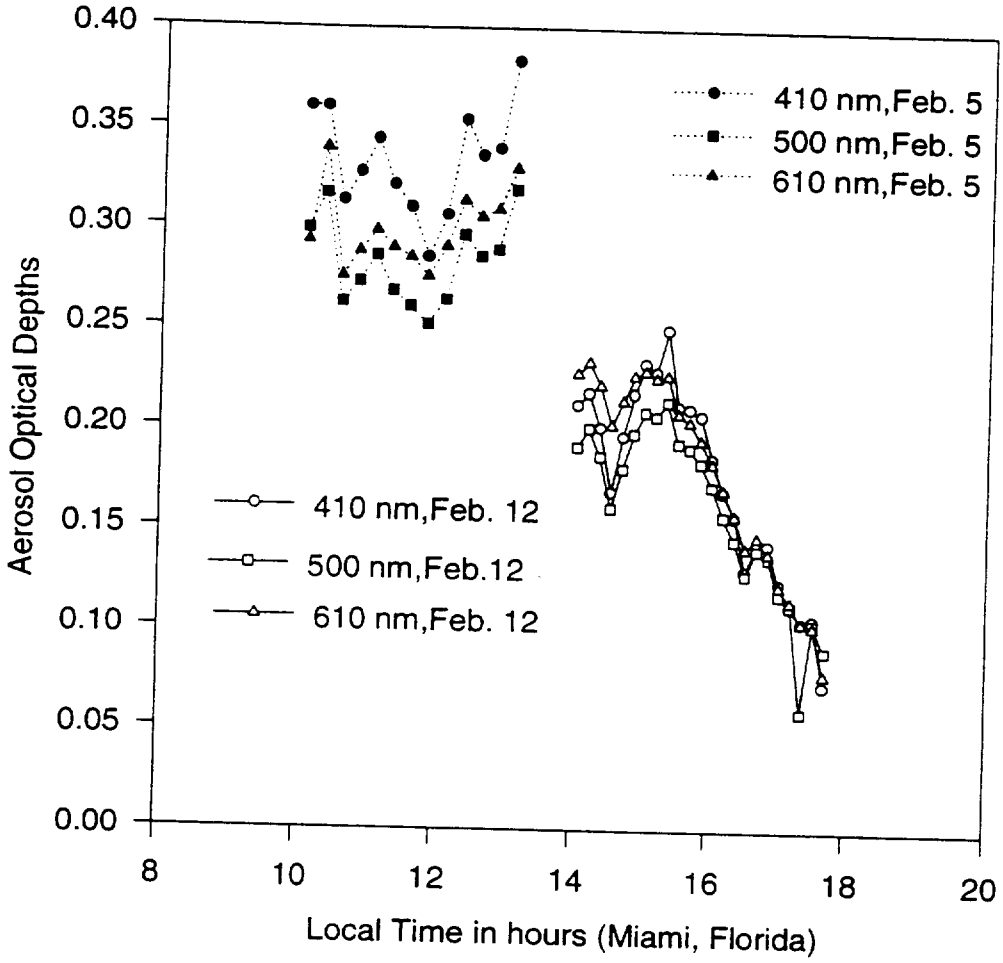
0.40
0.35
0.30
0.25
0.20
0.15
0.10
0.05
0.00
Aerosol Optical Depths
8
10
12
14
16
18
20
Local Time in hours (Miami, Florida)
410 nm,Feb. 5
500 nm,Feb. 5
610 nm,Feb. 5
410 nm,Feb. 12
500 nm,Feb.12
610 nm,Feb. 12

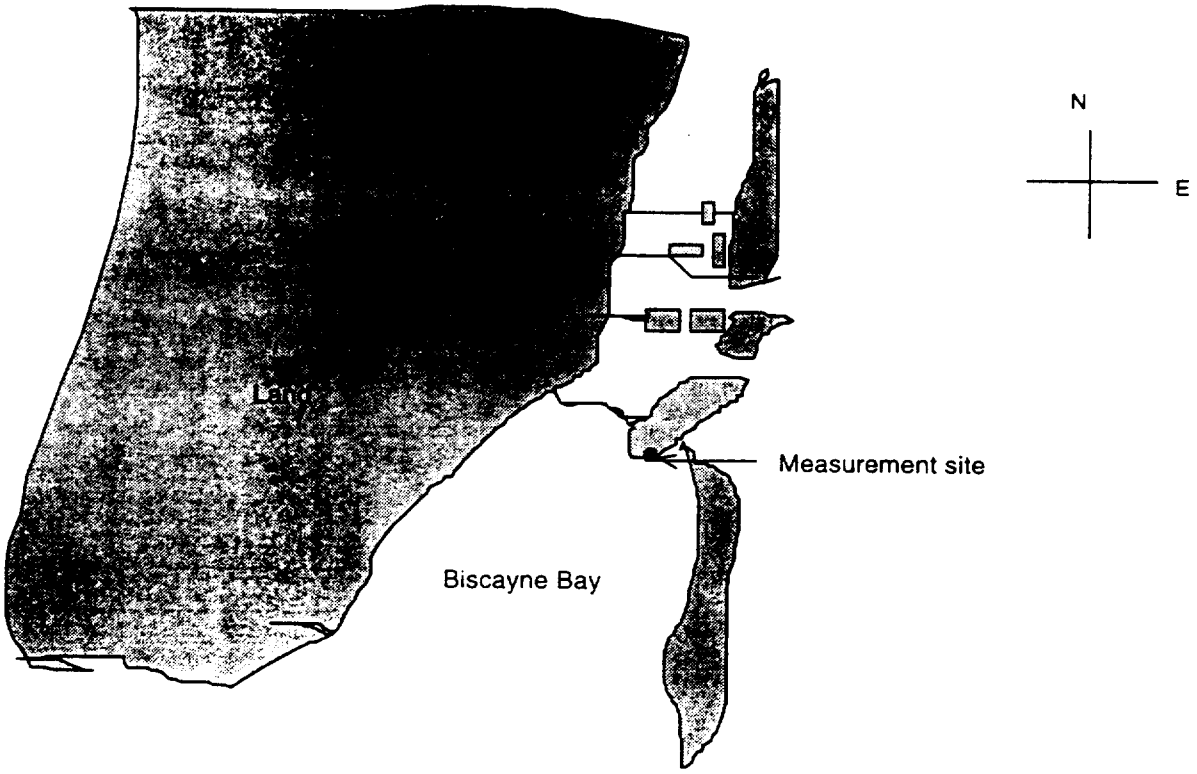
N
E
Land
Measurement site
Biscayne Bay

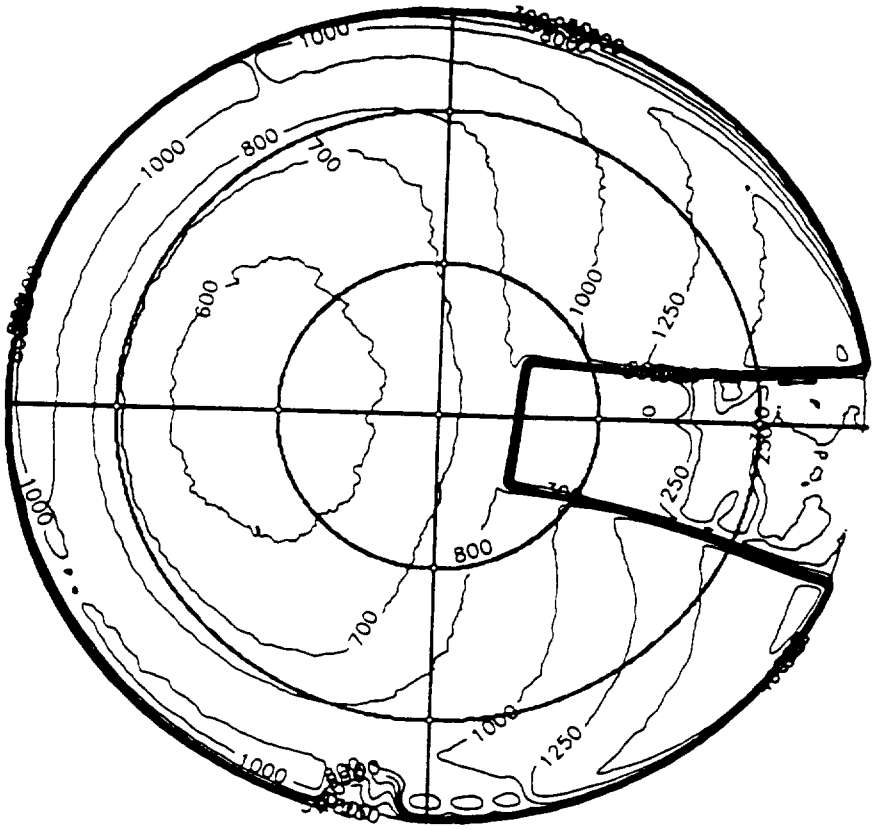
1000
800
700
600
1000
1250
0
250
800
700
1000
1250
1000
800

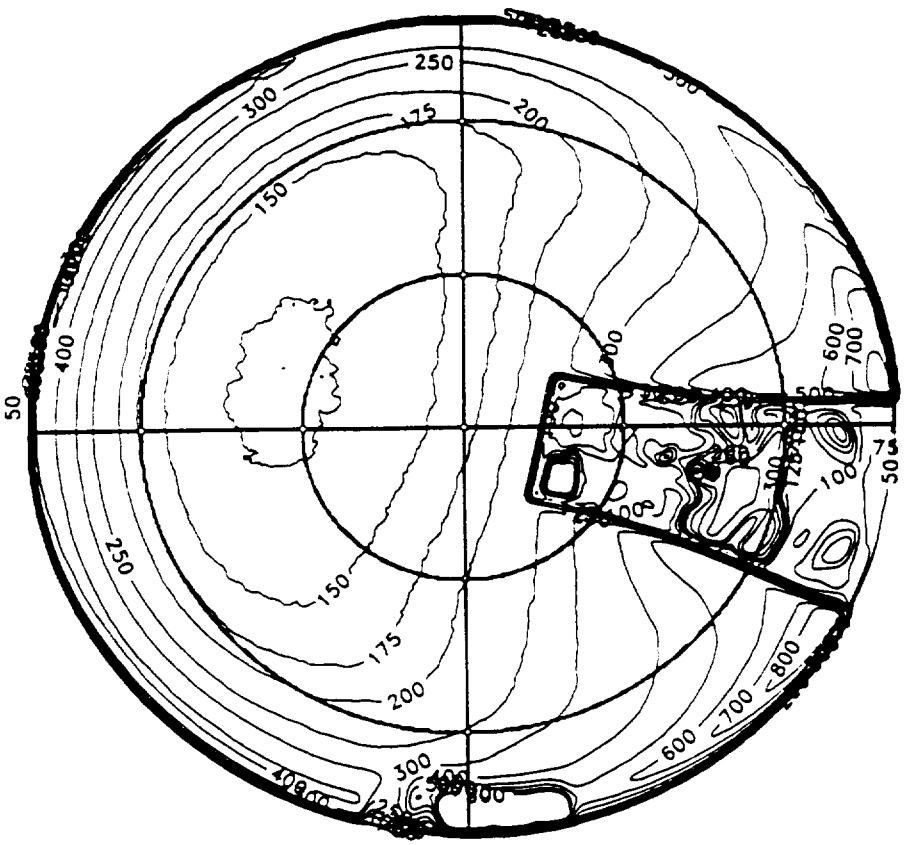
250
300
175
200
150
400
50
600
700
100
800
N

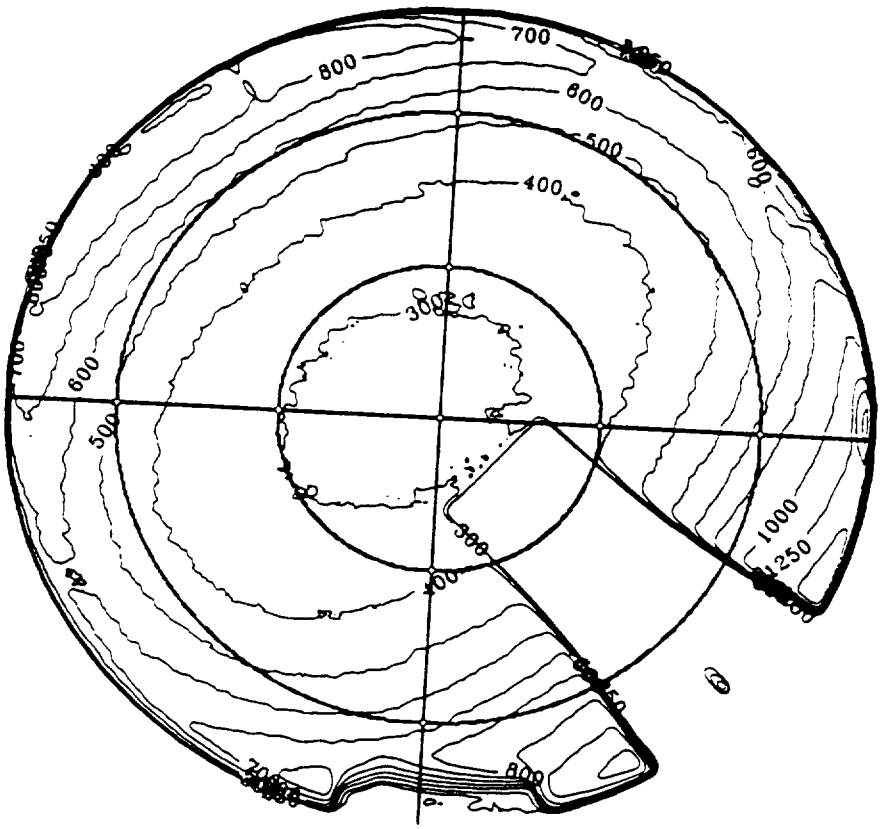
700
800
600
500
400
300
1000
250

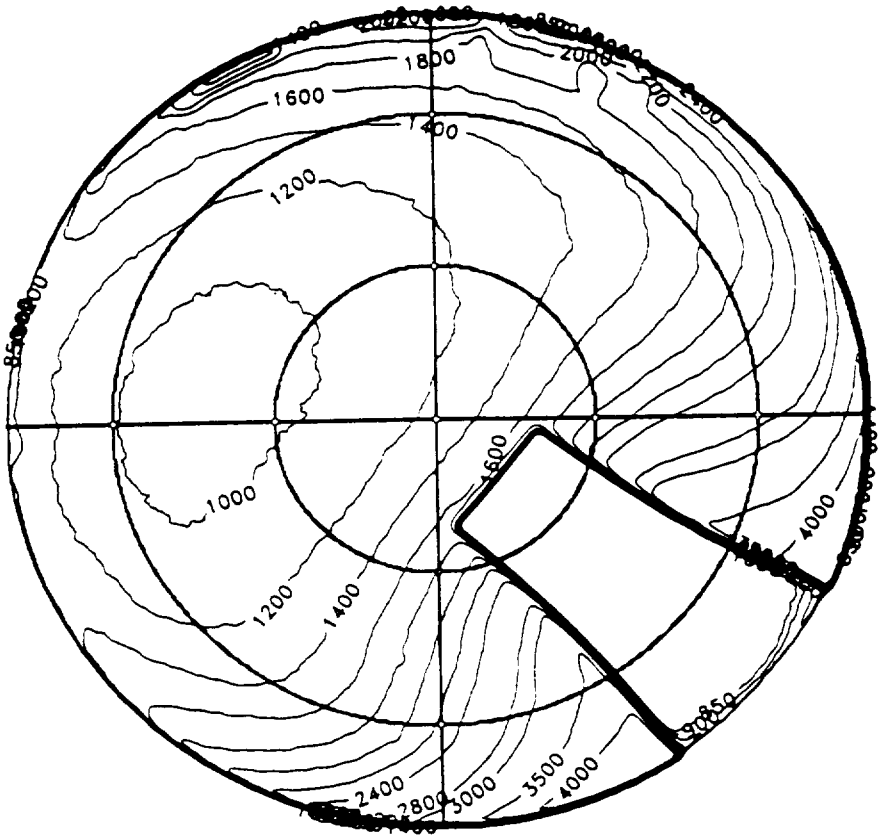
1800
1600
1400
1200
1000
1200
1400
1600
2400
2800
3000
3500
4000
4000

6a

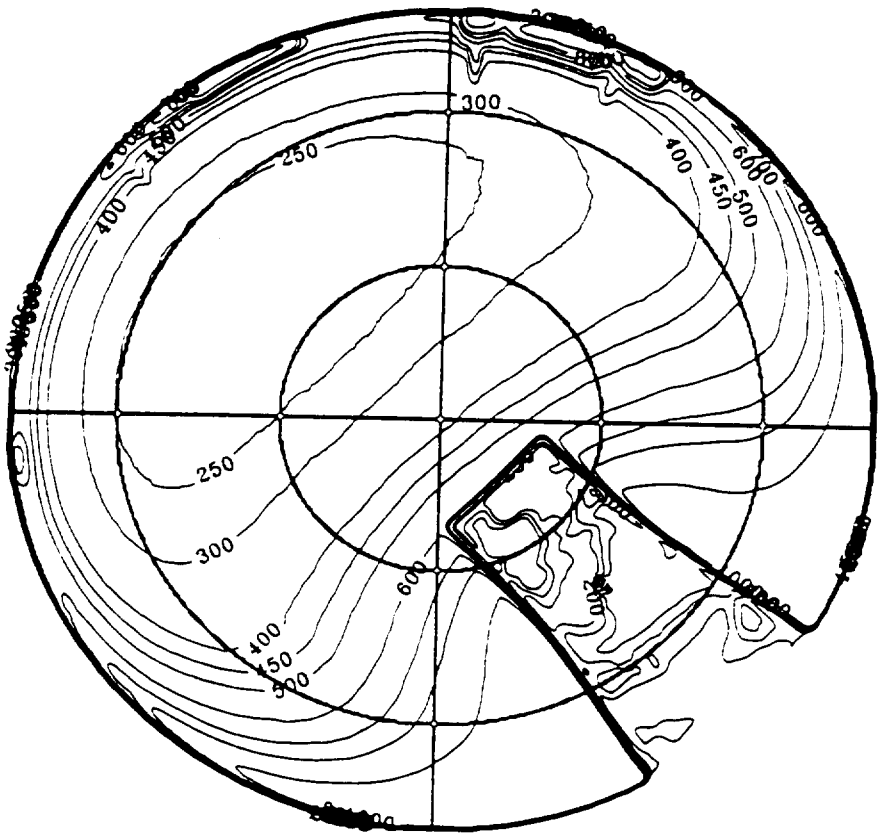
300
250
400
450
500
600
250
300
400
450
500

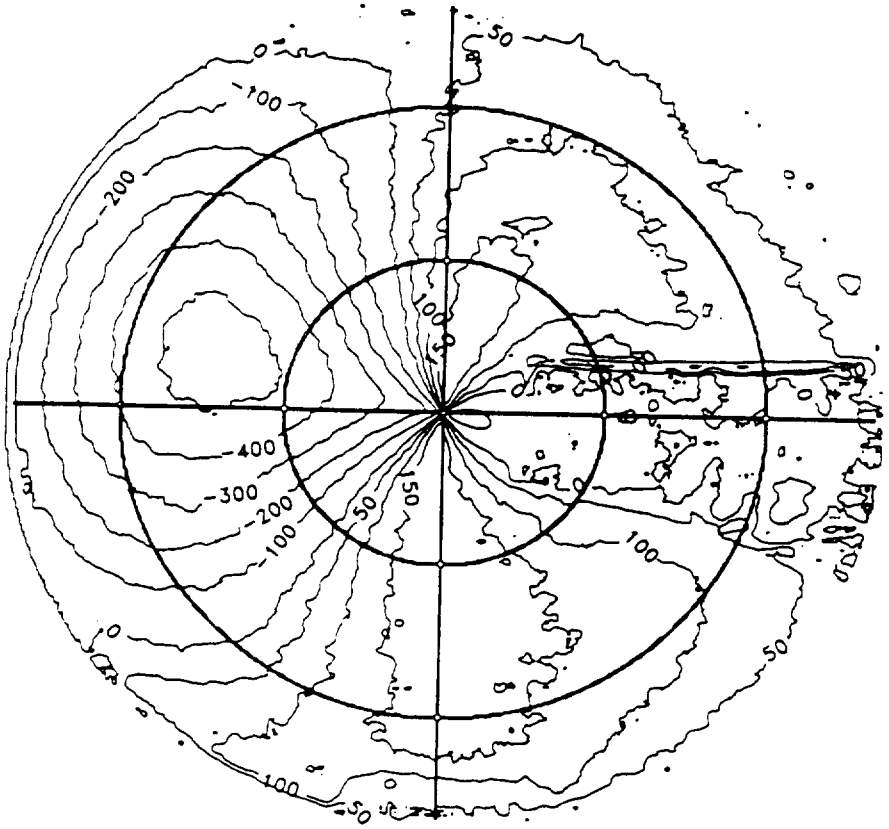
0
-100
-200
-50
-400
-300
-200
-100
-100
-50
150
50
100
0
50
-100
-50

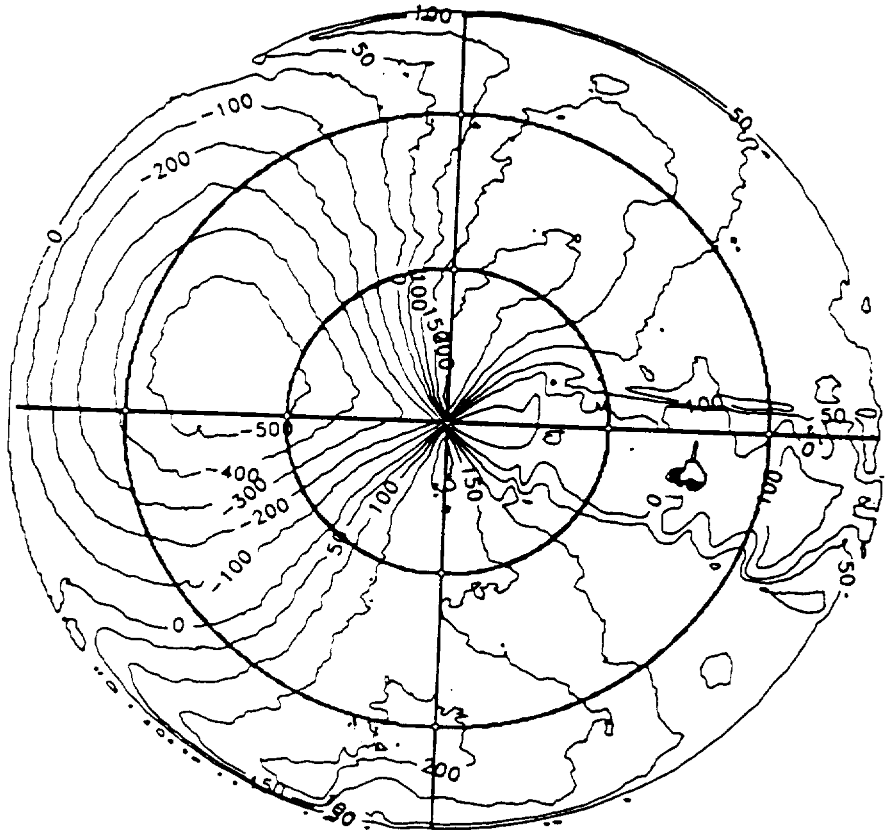

Liu & Vass Fig 7b

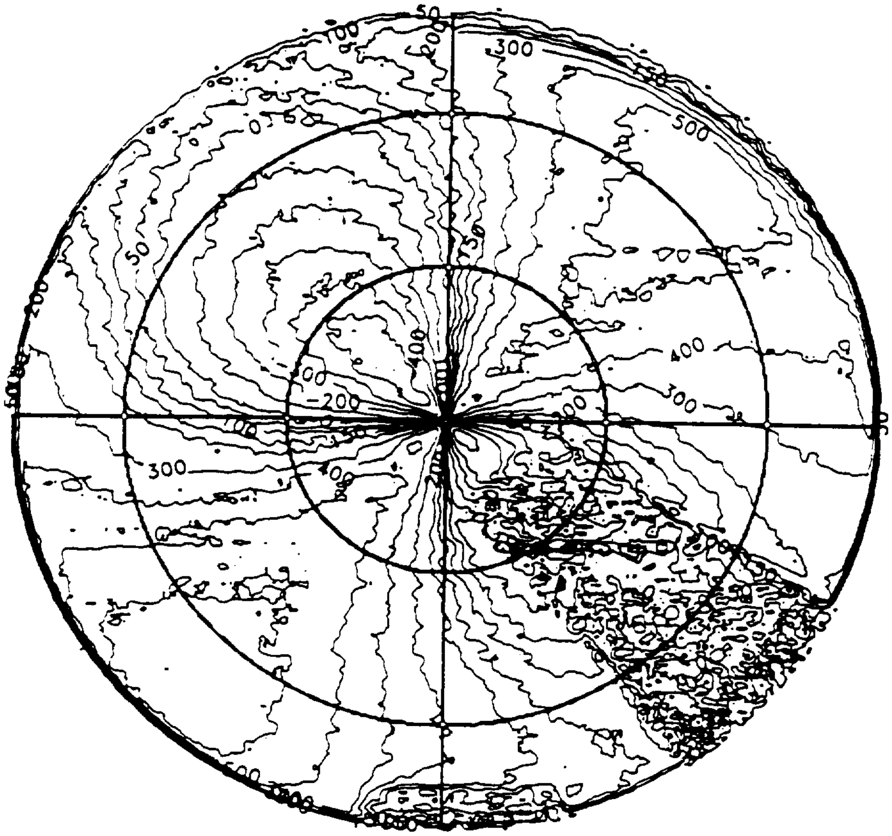

7c

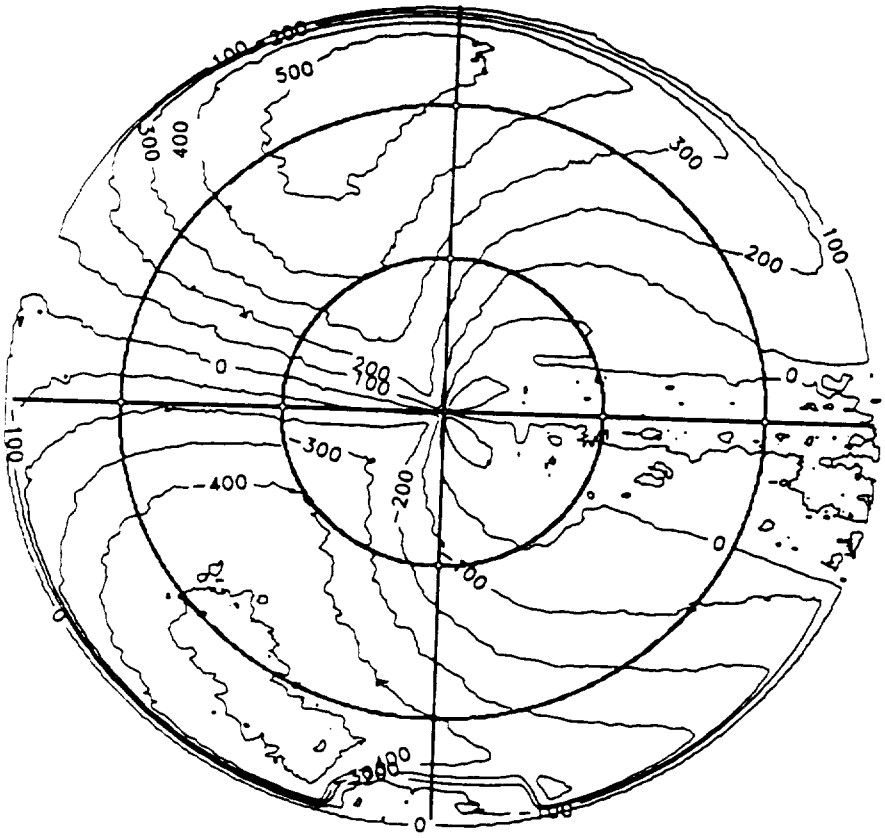

Lin x Vac Fig

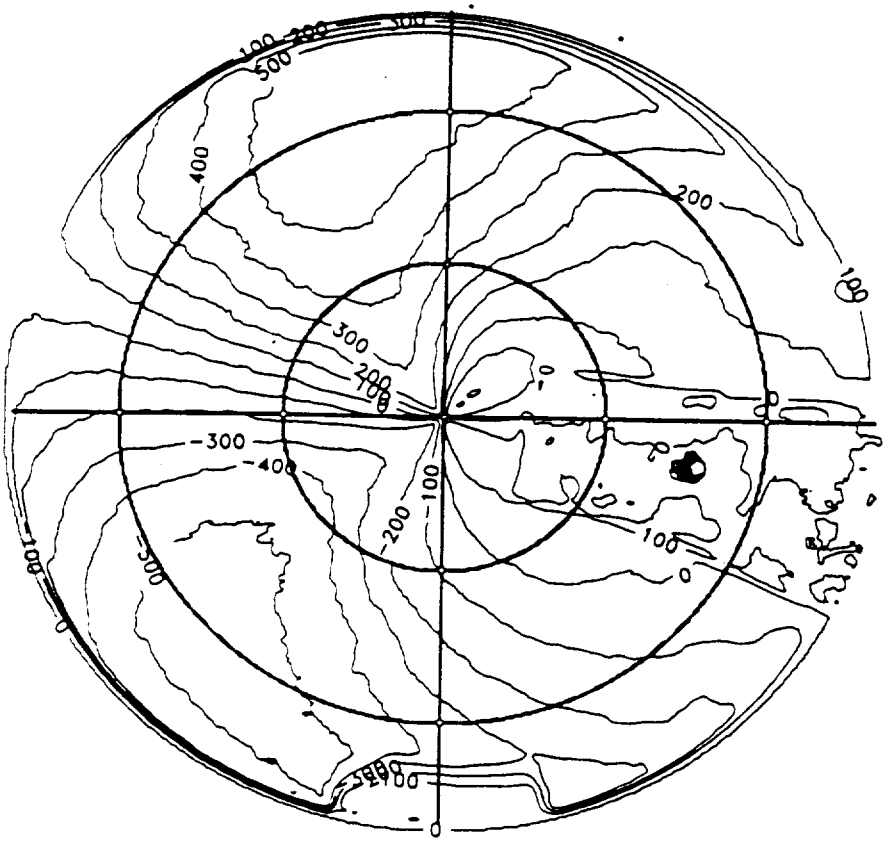

8b

Liu R Voss Fig. 8E

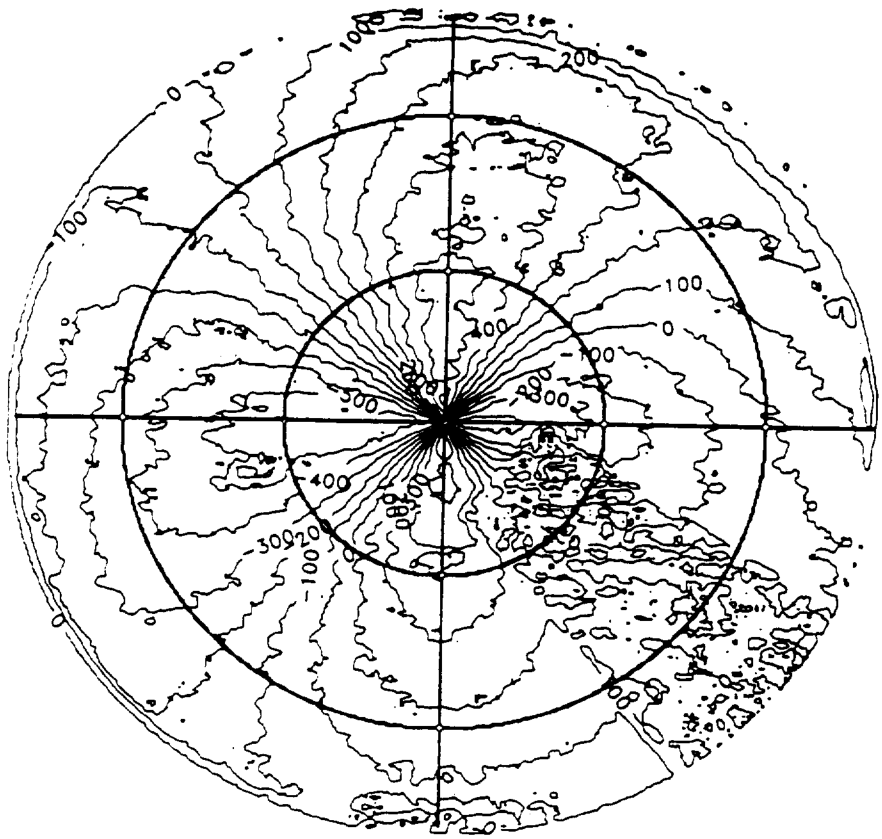

8C

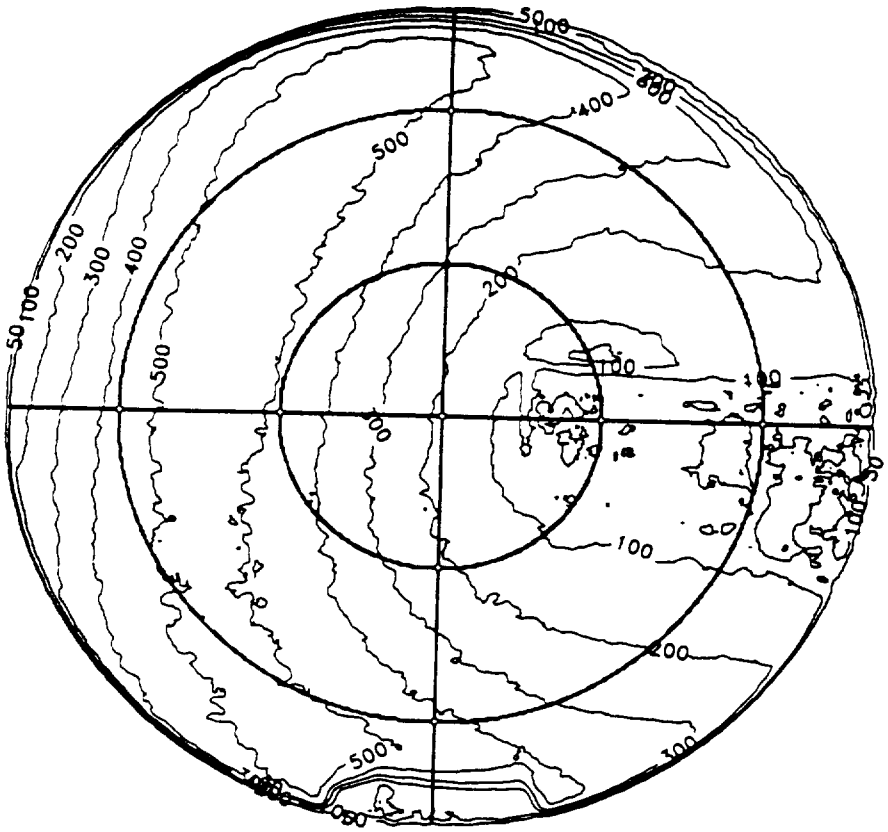
500
400
300
200
100
50
500
400
300
200
100
50
500
400
300
200
100
50

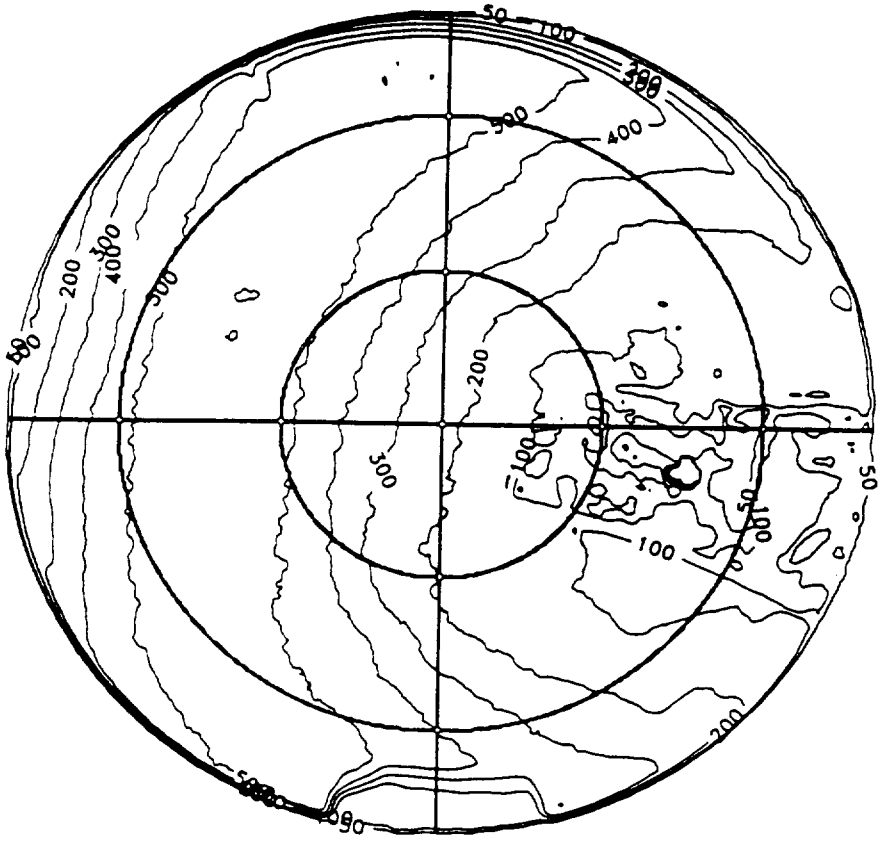
50
100
300
400
500
200
400
300
200
100
50
100
200
300
500
90

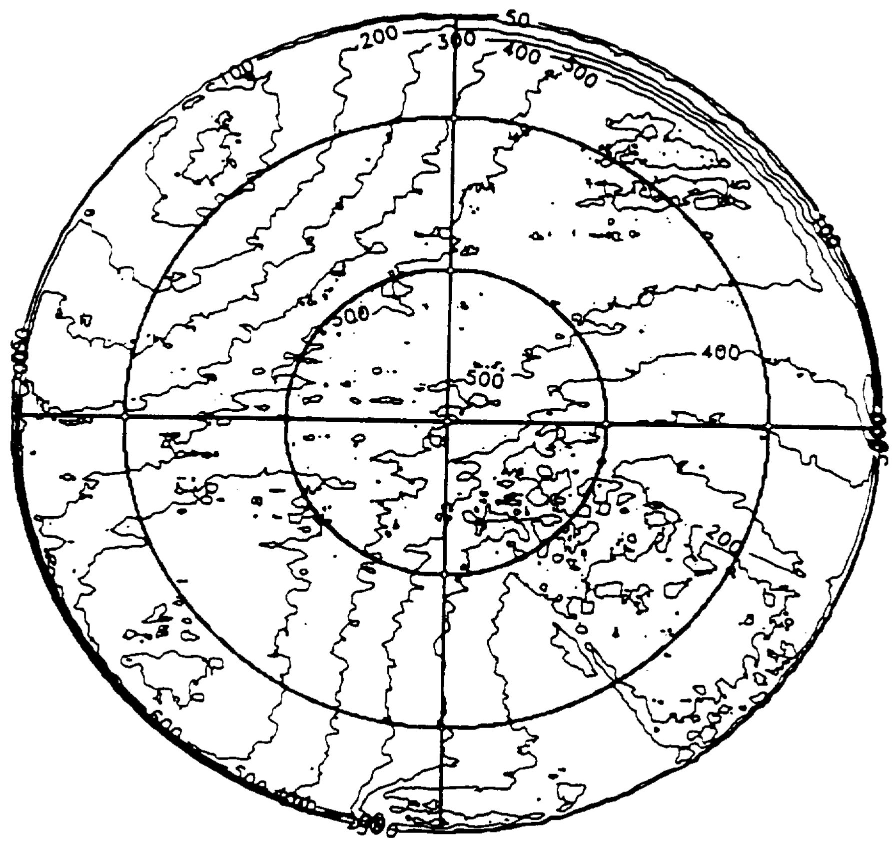

Liu & Vogt Fig 9S

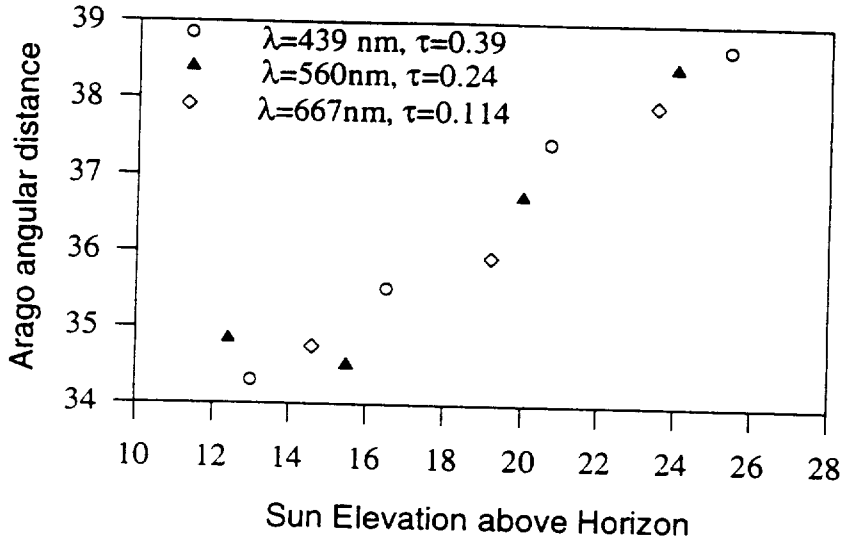
λ=439 nm, τ=0.39
λ=560nm, τ=0.24
λ=667nm, τ=0.114
Arago angular distance
Sun Elevation above Horizon
39
38
37
36
35
34
10
12
14
16
18
20
22
24
26
28

Lin & Voss

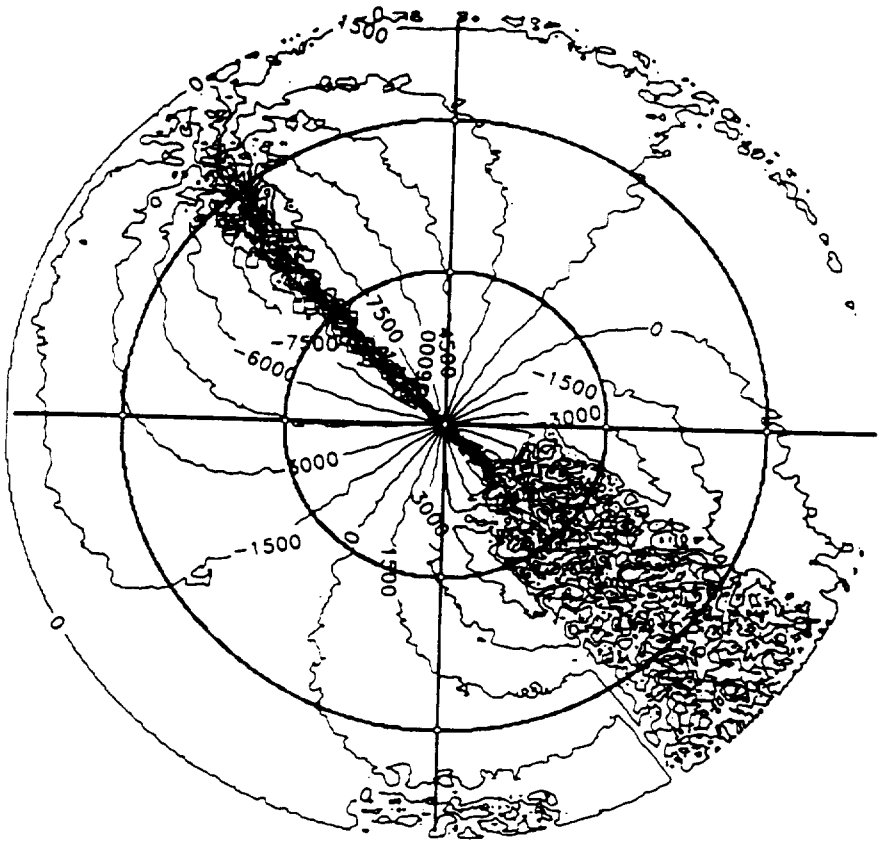
1500
0
-7500
-6000
7500
6000
-1500
3000
-6000
3000
-1500
0
-1500
0

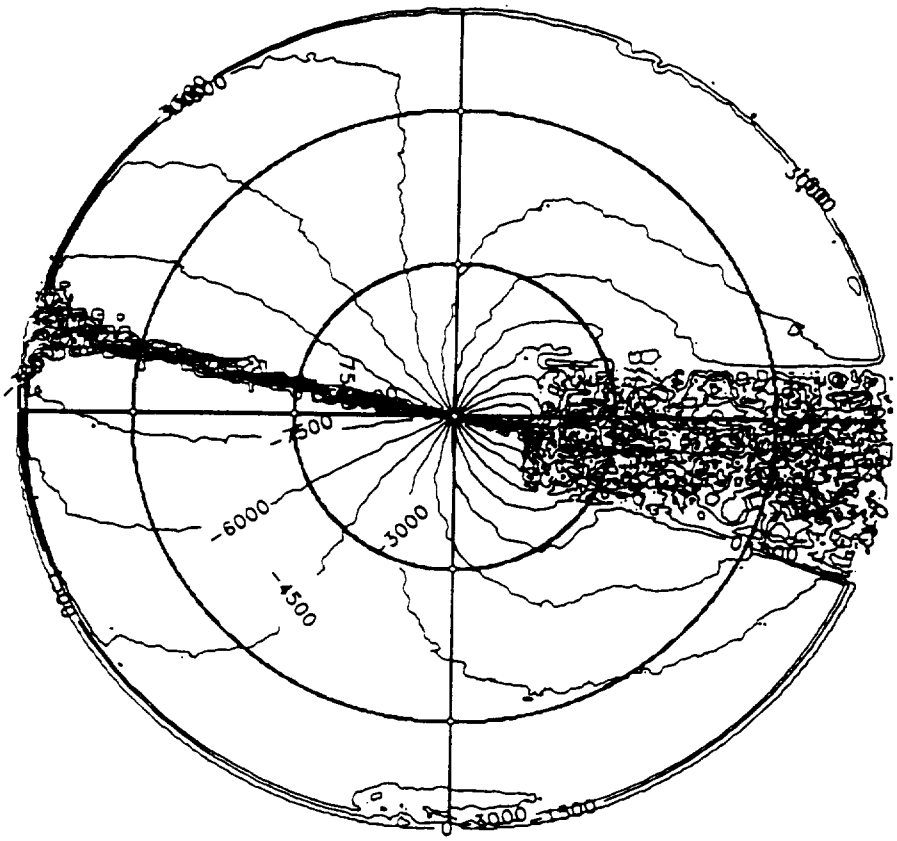
-7500
-6000
-4500
3000

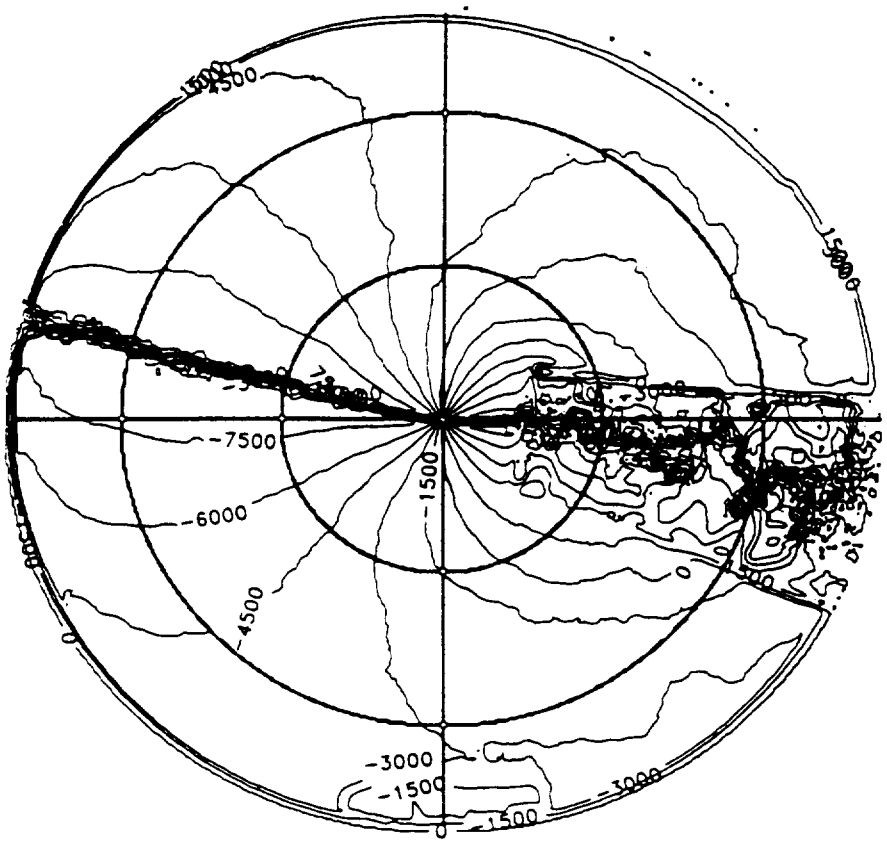

"b

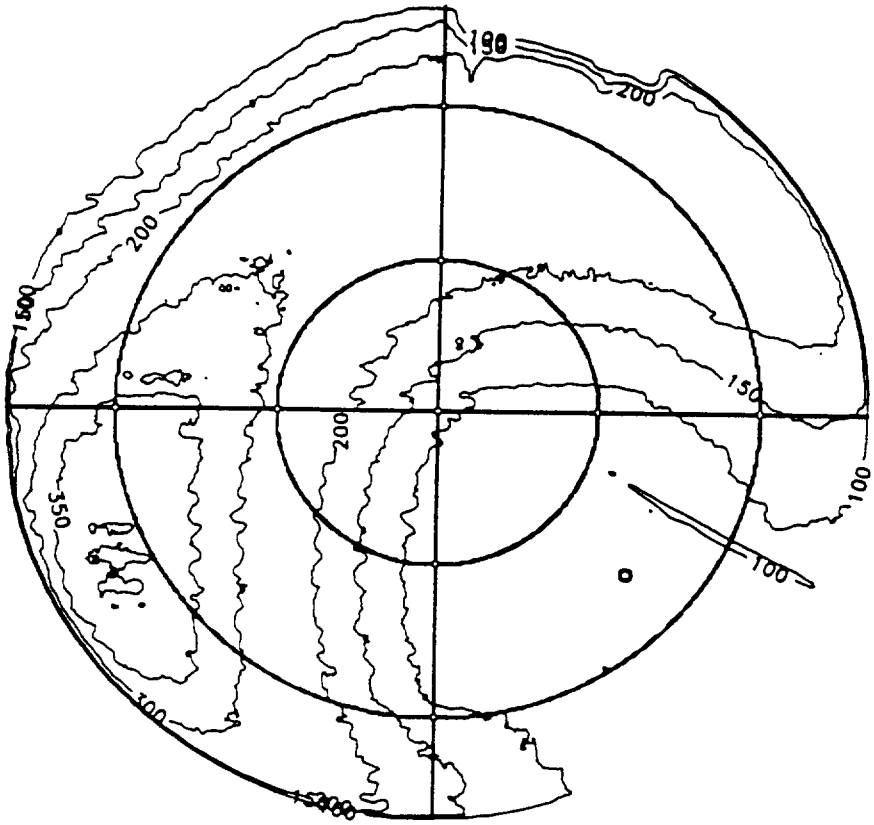
190
200
200
150
100
100
200
350
300

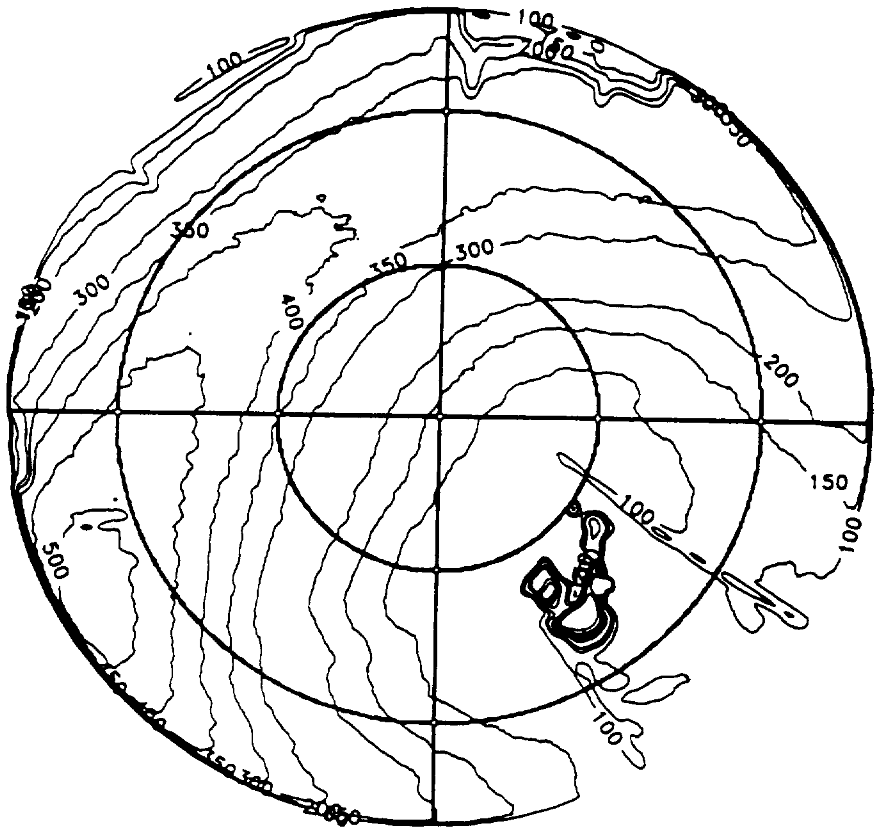

12b